

Quasi – Static Compression and Compression – Compression Fatigue Behavior of Regular and Irregular Cellular Biomaterials

Sunil Raghavendra¹, Alberto Molinari¹, Anni Cao², Chao Gao², Filippo Berto², Gianluca Zappini³, and Matteo Benedetti¹

¹University of Trento Department of Industrial Engineering

²Norwegian University of Science and Technology

³Lincotek Medical

November 25, 2020

Abstract

The main aim of the current study is to evaluate the compressive quasi-static and fatigue properties of titanium alloy (Ti6Al4V) cellular materials, with different topologies, manufactured via Laser Powder Bed Fusion (LPBF) process. The topologies herein considered are lattice based regular and irregular configurations of cubic, star and cross shaped unit cell along with trabecular based topology. The results have indicated that the effective stiffness of all configurations are in the range of 0.3 – 20 GPa, which is desirable for implant applications. The morphological irregularities in the structures induce bending dominated behavior affecting more the topologies with vertical struts. The S – N curves normalized with respect to the yield stress indicate that the behavior of star regular structures is between purely stretching dominated cubic and purely bending dominated cross based structures. Trabecular structures have shown desirable quasi-static and fatigue properties despite the random distribution of struts.

Quasi – Static Compression and Compression – Compression Fatigue Behavior of Regular and Irregular Cellular Biomaterials

Sunil Raghavendra^{1,*}, Alberto Molinari¹, Anni Cao², Chao Gao², Filippo Berto², Gianluca Zappini³, Matteo Benedetti¹

¹Department of Industrial Engineering, University of Trento, Via Sommarive 9, 38123 Trento, Italy

²Department of Mechanical and Industrial Engineering, Norwegian University of Science and Technology (NTNU), Richard Birkelands vei 2b, Trondheim 7491, Norway

³Lincotek Medical, Via Al Dos de la Roda, 60, 38057 Ciré-Pergine (TN), Italy

Abstract

The main aim of the current study is to evaluate the compressive quasi-static and fatigue properties of titanium alloy (Ti6Al4V) cellular materials, with different topologies, manufactured via Laser Powder Bed Fusion (LPBF) process. The topologies herein considered are lattice based regular and irregular configurations of cubic, star and cross shaped unit cell along with trabecular based topology. The results have indicated that the effective stiffness of all configurations are in the range of 0.3 – 20 GPa, which is desirable for implant applications. The morphological irregularities in the structures induce bending dominated behavior affecting more the topologies with vertical struts. The S – N curves normalized with respect to the yield stress indicate that the behavior of star regular structures is between purely stretching dominated cubic and

purely bending dominated cross based structures. Trabecular structures have shown desirable quasi-static and fatigue properties despite the random distribution of struts.

Keywords: Cellular materials, LPBF, Titanium alloy, Compression, Fatigue loading, Strength.

Nomenclature

AM: Additive manufacturing

CE: Chemical Etching

C_1, C_2, m : S-N curve fitting parameters

HIP: Hot – isostatic pressing

LPBF: Laser powder bed fusion

n: Number of data points in fatigue

p: Number of curve fitting parameters

S^2 : Scatter of fatigue data

E_m : Monotonic Young’s modulus

E_c : Cyclic Young’s modulus

ρ_s : Density of cellular specimen

ρ_o : Theoretical density of Titanium

σ_y : 0.2% offset yield strength

σ_{mc} : Maximum compressive strength

σ_{max} : Maximum stress (fatigue)

σ_{max-i} : i^{th} maximum stress (fatigue)

σ'_{max-i} : estimated i^{th} maximum stress (fatigue)

Introduction

The current trends in aerospace, automotive and bio-medical industries involve the development of optimized light-weight structures providing high strength as close as possible to that of conventional bulky structures¹. Also, foam based cellular materials have been extensively used in energy absorption applications. However, one of the limitations to use these structures is the poor availability of control on the parameters such as pore size and wall thickness which determine their properties. The development of lattice based cellular materials with repetitive unit cells has been helping to tailor the mechanical properties based on the loading requirements. Cellular materials are termed as true cellular materials when their relative density is less than 0.3².

Cellular materials become a rising star in the biomedical industry and are a prospective replacement for fully solid implants. The use of solid implants which have higher stiffness compared to the surrounding bone results in stress shielding phenomenon, which might cause bone resorption. This eventually results in implants loosening which requires implant replacement^{3,4}. The use of porous cellular materials helps to adapt the implants stiffness to that of the surrounding bone. Also, the presence of pores in the structure improve bone regeneration which provides better fixation^{5,6}. Metal alloys being the first choice for implants, Titanium alloys such as Ti6Al4V have been widely used in implants manufacturing due to their high strength, corrosion resistance and bio-compatibility⁷⁻⁹.

Additive manufacturing (AM) technologies such as Laser powder bed fusion (LPBF) facilitates the production of intricate complex structures in a short period of time. The same technique is employed in the current study. LPBF is widely used in the production of cellular materials to obtain higher precision compared to other AM techniques^{5,10}. The LPBF fabricated parts have certain issues such as quite low surface finish, internal porosity, geometrical deviation, residual stress and brittle material phases, which negatively affect the mechanical properties of the structures. Various studies have concluded that the above-mentioned issues are highly influenced by process parameters such as laser power, hatching distance, scanning speeds and building direction^{11–16}. Furthermore, heat treatment processes such as stress relief and hot-isostatic pressing significantly improves the mechanical performance by transforming the microstructure to a more stable ductile $\alpha+\beta$ phase with the additional advantage of eliminating residual stresses and internal porosity^{17–21}.

The mechanical properties of cellular materials are mainly characterized by material type, cell topology, and relative density. Their characterization is generally carried out through static and fatigue compression tests. Cheng et al.²² compared compressive properties of foam based and lattice based cellular structures with different relative densities, indicating that the lattice based structures had higher specific strength. Additionally, various studies focusing on the influence of different types of unit cell and relative density on the compressive behavior of cellular materials were carried out^{23–30}. It was reported that the strength and stiffness of the structures enhances with increasing the relative density in well agreement with Gibson-Ashby law². This increase depended on the morphology of the unit cell as well. Depending on the local loading conditions in the struts, the unit cell topologies can be grouped into two different categories of bending dominated and stretching dominated structures. Stretching dominated structures are characterized by high strength and stiffness since the struts are subjected to axial loading conditions. On the other hand, bending dominated structures do not possess any struts along the loading direction and hence fail due to bending loads in the struts. Bending dominated structures are more compliant compared to stretching dominated structures which failed mainly due to buckling. The compressive behavior of bending dominated structures consist of three regions, elastic region, flat plateau region where strain increases with constant stress followed by densification. However, in stretching dominated structures, the plateau region consists of oscillating stress followed complete densification of the structure despite cell morphology^{29–34}.

Cellular materials used in biomedical applications as well as aerospace applications are exposed to cyclic loads. Therefore, understanding the fatigue behavior of these materials has gained strategic importance in the recent years. Various studies have indicated that the compression-compression fatigue properties are dependent on various parameters such as cell topology, stress ratio (R-ratio), heat treatment and the presence manufacturing defects from AM process^{20,29,35–42}. Zhao et al.³⁶ and Yavari et al.³¹ have investigated the effect of cell topology and porosity on the compression-compression fatigue behavior. The studies have clearly shown that if the deformation in the structure is bending dominated, plastic strain is progressively accumulated, leading to the final fatigue failure. While the fatigue crack growth is decelerated in structures that fail due to buckling. The S-N curves normalized with respect to the yield stress indicate that a single power law is followed by a particular cell topology despite the difference in porosity. The effect of fatigue the stress R-ratio has been studied using diamond unit cells. Specifically, it was found that the higher the stress R-ratio the lower the fatigue strength at a given number of cycles to failure⁴³. The effect of post manufacturing thermal and chemical treatments on fatigue properties were also studied. Yuan et al.⁴⁴ used two heat treatment temperatures (750^oC and 950^oC) and showed that samples treated at 950^oC had a broader plateau under static loading indicating better performances under plastic strains. The fatigue endurance ratio was increased by 0.5 – 0.6 times with heat treatment at 950^oC. Hot-Isostatic pressing (HIP) and Chemical Etching (CE) treatments have improved the fatigue strength of cellular materials by increasing the ductility, eliminating some internal defects and improving the surface finish²⁰. The fatigue failure of cellular materials can be divided into strain accumulation, crack initiation and crack propagation. The strain accumulation in the structures is mainly due to cyclic ratcheting as indicated in various studies³⁶. The crack propagation takes place in two steps, a first propagation in the struts followed by propagation through the unit cells⁴⁵. Applied stress level and surface defects such as roughness, defects and waviness have a greater influence on the fatigue properties compared to internal porosity in the crack initiation stage.

On the other hand, parameters such as material, microstructure and internal porosity influence the crack propagation phase^{38,46}.

The porous material used for bone implants should have mechanical properties in range of the human bone for better fixation. Therefore, mechanical properties of the implants are of primary importance at the initial stage of implant fixation; once the bone regeneration is complete, higher fatigue life from the implant may not be necessary³⁵. Hence, it is necessary to study a variety of structures with varying cell topologies, irregularities, and pore shape to understand the material properties. Benedetti et al.⁴⁷ analyzed the compressive behavior of various types of cellular materials in presence of different porosity levels. That study has shown that the properties of the different analyzed structures range between the two extremities of a cubic structure and a cross shaped cellular structure. Also, despite the absence of vertical struts, cross shaped samples had the highest strength for the given stiffness. Therefore, the below mentioned seven different topologies are considered in the present study to explore their suitability to be used as an osteo-integrative coating for solid implants. Since this porous coating is commonly placed in the contact region between bone and solid implant, the resulting load is entirely compressive. Therefore, the knowledge of monotonic properties and fatigue strength under compressive loads is fundamental for their proper design. For this purpose, cellular lattice specimens were manufactured via LPBF using the titanium alloy Ti6Al4V. Their cell architecture includes three regular structures ((#1) Cubic, (#2) Star and (#3) Cross, three irregular structures obtained by skewing the junction of regular structures ((#4) Cubic irregular, (#5) Star irregular and (#6) cross irregular); a (#7) trabecular consisting of random arrangement of struts mimicking trabecular bone topology structure. The samples were analyzed for assessing porosity and struts dimensions. Compression tests have been carried out using monotonic and cyclic loading conditions to obtain the strength and stiffness properties (under loading and unloading) of the considered structures. The specimens have been subjected to compression-compression fatigue loading with an R-ratio of 0.1 and loading between 0.1-0.8 yield load. One specimen from each topology has been employed to visually detect the deformation pattern in the different investigated structures. Fracture surface analysis has been carried out to show the failure mechanisms under quasi-static loading and cyclic loading. The effect of geometrical irregularity on the fatigue performance has been explicitly shown in the normalized S-N curves. The results of the regular and irregular topologies have been carefully compared with the trabecular based topology for a better understanding of their behavior with the future optic of possible systematic employment in biomedical applications.

Materials and Methods

This section gives the detailed description of the manufacturing process, specimen design and experimental method employed in the present study.

The cellular materials were fabricated via LPBF technology using an EOS machine equipped with a 400 W laser, at the Lincotek Medical facility, Italy. The samples were manufactured by using a biomedical grade titanium alloy (Ti6Al4V) powder with particle size in the range of 15-45 μm and with a layer thickness of 60 μm . All the specimens were then subjected to heat treatment under proprietary conditions to transform the as-built α' -martensitic microstructure into a stable $\alpha+\beta$ phase and to relieve the residual stress from the LPBF process.

Manufacturing and Specimen Design

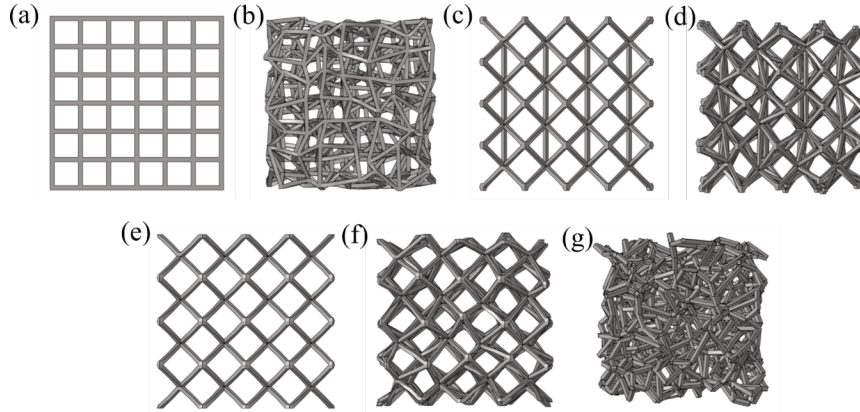


Fig.1 Schematic representation of the topology of studied cellular structures, XY view; (a) Cubic regular, (b) Cubic irregular, (c) Star regular, (d) Star irregular, (e) Cross regular, (f) Cross irregular, (g) Trabecular.

In the present study, 7 different topologies with a target strut thickness of 500 μm and a target pore size of 1100 μm were selected. The XY view of the topologies considered are as shown in Fig. 1, and the samples were printed along the Y direction. The regular structures were named as cubic, star and cross. The irregular structures were named as cubic irregular, star irregular and cross irregular. Irregular structures were obtained by using an algorithm to misalign the nodes of the regular structures in random directions and distances to induce irregularity. Trabecular is a modified version of the Voronoi tessellation with a narrow pore distribution. This structure is able to mimic the trabecular human bone and consists of 4 to 6 struts joined at a node and oriented in random directions. The number of struts at a node and their orientation depend on the cell topology.

Cylindrical test specimens of 15mm diameter (d) and 17mm height (h) ($h/d > 1$) were used both for quasi-static and fatigue tests. The top and bottom surfaces of the specimens were polished to make sure the contact surface is flat for fatigue testing.

Experimental Procedure

Microstructure

The microstructure of the specimen was observed along the XZ plane (parallel to printing plane) and XY plane (perpendicular to the printing direction). One cubic regular specimen was cut along two planes and subjected to polishing process with SiC abrasive papers of different grit size from 220 to 2400, 3-micron diamond solution, and finally polished with alumina suspension to give it a mirror finish. The samples were then etched using a Kroll's reagent to reveal the microstructure.

Porosity and Geometrical Deviation

The porosity was calculated on the compression test samples (5 specimens) using equation 1, where ρ_s is the density of the specimen and ρ_o is the theoretical density of Ti6Al4V alloy (4.42 g/cm^3)⁴⁸. Specimen density was calculated using the mass of the specimen obtained from gravimetric precision balance (XS Balance (BL 224), Italy) and the nominal volume calculated using the height and diameter of the specimen.

$$\text{Porosity} = \frac{\rho_o - \rho_s}{\rho_o} \dots \dots (1)$$

The geometrical deviation of structures was carried out to obtain the thickness of different struts. The struts in all seven topologies can be categorized into horizontal struts, vertical struts, oblique (inclined struts)

(struts in regular structures), random and irregular struts (struts in irregular structures). The images of the different topologies were captured using a stereo optical microscope (Nikon SMZ25) as shown in Fig.2. The strut thickness was measured from end to end including the roughness on the surface using ImageJ® software. To obtain a statistically significant data, 100 measurements were captured for all the different categories of struts mentioned above.

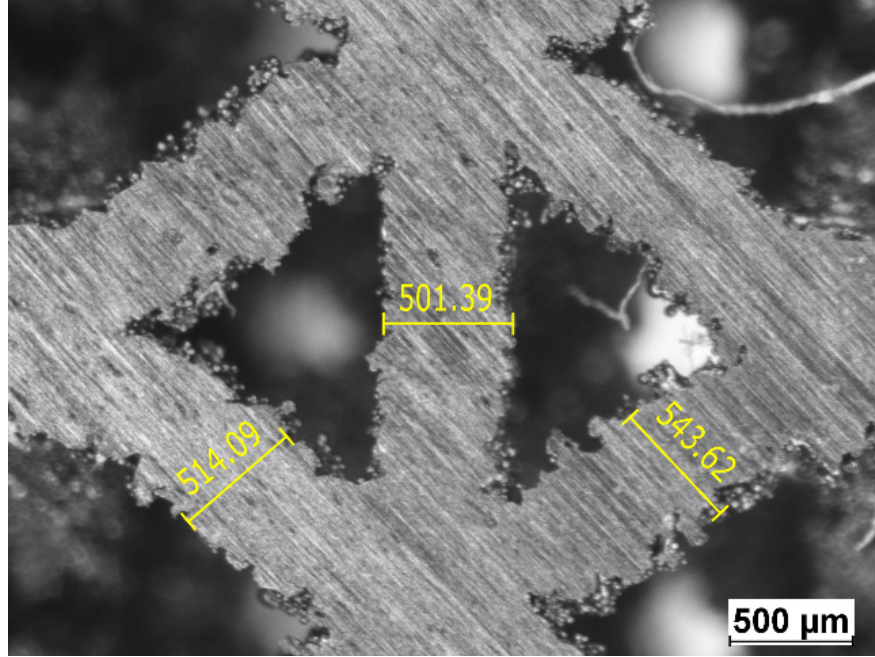


Fig.2 Spectro microscopy images for strut thickness measurement (a) Cubic Irregular (b) Star Regular with thickness measurement in μm .

Quasi-static and fatigue testing

The mechanical tests were carried out under two loading conditions, monotonic quasi-static and cyclic. They were carried out according to the standard ISO 13314:2011 for metallic foams⁴⁹. Both tests were carried out at room temperature using an INSTRON universal testing machine with a load capacity of 100kN. The displacement was measured using an Instron LVDT. A constant crosshead speed of 1mm/min and a data sampling frequency of 1kHz was employed. For each configuration, one specimen was tested under monotonic compression condition and four specimens under cyclic condition.

The stress-strain curve obtained from the monotonic testing condition is then used to acquire the monotonic Young's modulus (E_m), 0.2% offset yield strength (σ_y) and the maximum compressive strength (σ_{mc}). Cyclic tests were performed to obtain the cyclic Young's modulus (E_c) after stabilization of the stress-strain response. The specimens were loaded between 20-70% of the yield load obtained from the monotonic testing condition using a triangular shape wave for five cycles.

High cycle compression-compression fatigue testing was carried out for a minimum of 12 specimens for each topology. RUMUL resonating fatigue test machine was used with an R-ratio of 0.1 in compression. The applied maximum load was chosen in the range 0.1-0.8 yield load to obtain the S-N curves^{36,50}. It was verified that the contact surfaces of the specimens were flat with no irregularities. A frequency drop of 1 Hz during the test was considered as an indicator of fatigue failure in the specimens, and the number of cycles at that specific moment was recorded as fatigue life. The S-N curve was subsequently obtained by fitting the data points using a curve fitting expressed by equation 2, where σ_{\max} is the maximum stress, N_f is the number of

cycles to failure, and C_1, C_2, m are the curve fitting parameters. The run-out condition for the specimens was set as 10^7 cycles and the fatigue strength of the specimens was calculated at 10^6 cycles using the S-N curves. The scatter of the fatigue data (S^2) is calculated by equation 3, where $\sigma_{\max-i}$ is the i^{th} maximum stress, $\sigma'_{\max-i}$ is the i^{th} estimated maximum stress, n is the number of data points and p is the number of parameters in equation 2 and the standard deviation of the fatigue strength was calculated as indicated in the reference¹⁸. Investigation of the fractured surface was carried out by using a JOEL JSM-IT300LV scanning electron microscope.

$$\sigma_{\max} = C_1 + \frac{C_2}{(Nf)^m} \dots\dots\dots (2)$$

$$S^2 = \frac{\sum_{i=1}^n (\sigma_{\max-i} - \sigma'_{\max-i})^2}{n-p} \dots\dots\dots (3)$$

To obtain the deformation mechanism and the crack propagation planes characterizing any cellular structure considered herein, some dedicated fatigue tests were carried out at a frequency of 5Hz using an MTS 809 Axial/Torsional test system with a load capacity of 100 kN. To evaluate the failure sequence during the fatigue loading, a high speed camera with a capturing frequency of 30 Hz was used to record the whole duration of the fatigue tests. The frames from the captured video have been indicated in the results and discussion section.

Results and Discussion

Microstructure

Ti6Al4V parts manufactured using LPBF process are characterized by an α' martensitic phase due to the rapid cooling, which makes the material brittle⁵¹. This brittle nature of martensitic phase can be detrimental to fatigue properties of the part due to its higher susceptibility to voids and surface defects. However, the specimens considered in this study were subjected to heat treatment after the manufacturing process. This heat treatment transforms the brittle α' to a more ductile $\alpha+\beta$ phase. The microstructure of the LPBF specimens was obtained in two different planes as shown in Fig.3. A uniform basket-weave microstructure was obtained with $\alpha+\beta$ lamellae phase, indicating a significant change in the microstructure from the heat treatment process in Fig.3(a).

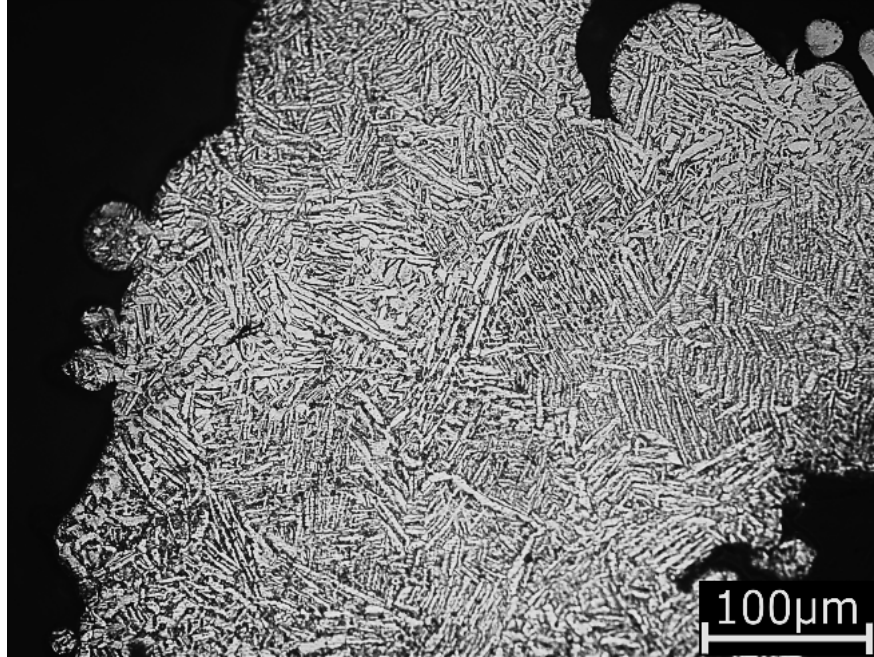


Fig.3 Microstructure of strut cross section (a) XY plane (b) XZ plane

Porosity and Geometrical deviation

Table 1 Measured porosity for all topologies

Sample	Cubic Regular	Cubic Irregular	Star Regular	Star Irregular	Cross Regular	Cross Irregular	Trabecular
Porosity	76 ± 0.15	71 ± 0.21	77 ± 0.32	77 ± 0.18	79 ± 0.18	80 ± 0.19	71 ± 0.32

The measured porosity values was calculated as described in section 2.2.1. Star and cross based specimens had the highest porosity values, while the trabecular structures had the lowest porosity. The variation in porosity is related to the thickness variation in the struts oriented in different directions. This clearly indicates the effect of strut orientation on the overall porosity of the investigated structures. The thickness variation in struts with different orientations are explained below.

The strut thickness was measured as described in the section 2.2.2. The average strut thickness is as shown in Fig.4a. The horizontal struts have the lowest thickness ($\sim 370 \mu\text{m}$) while random structures have the highest measured thickness ($\sim 600 \mu\text{m}$). The probability distribution curve shown in Fig.4b displayed a normal distribution. During the printing process, the laser penetrates into a layer below to induce perfect fusion of metal. But in the case of horizontal struts, due to absence of support, the laser also melts the powder from a layer below the first layer. This induces irregularity and sagging in the struts. Due to this, the thickness of horizontal struts varied from $280 \mu\text{m}$ to $450 \mu\text{m}$. However, when comparing vertical and oblique struts, the average thickness is close to each other, however the distribution indicates that the vertical struts were uniform when compared to oblique struts. The presence of complete support in vertical struts layer during the melting process made the strut uniform. Irregular struts had a similar distribution compared to oblique struts but with a shift in the average thickness by $20 \mu\text{m}$. Random struts in trabecular specimens are thicker due to overlapping of struts, especially at the junctions which reduce the porosity of the samples.

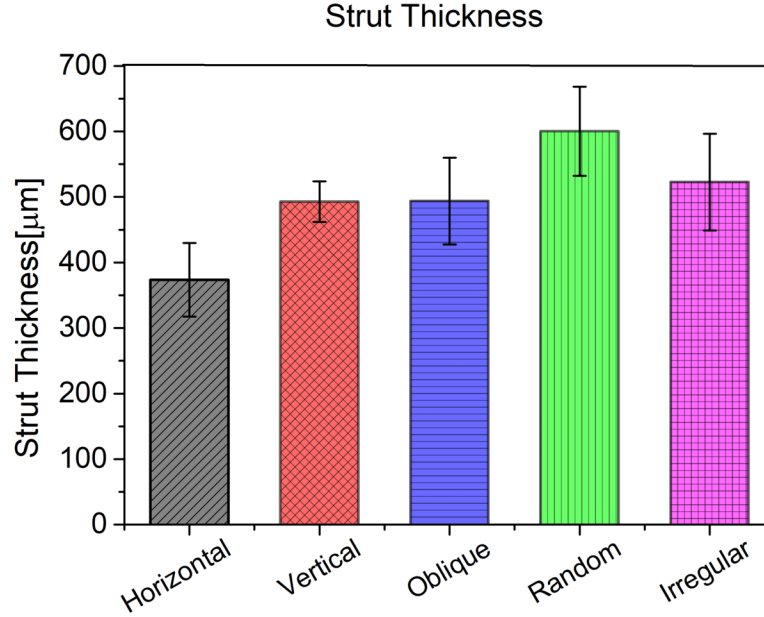


Fig. 4 (a) Measured strut thickness (b) Normal distribution of measured strut thickness for different strut orientation

Relating the strut thickness to porosity, the random struts had the highest thickness and hence trabecular structures had the lowest porosity. Cross based structures with oblique struts had the highest porosity, followed by star based structures which had one extra vertical strut when compared to cross based structures. But, the thickness difference in the horizontal and irregular struts can be clearly seen when comparing the porosity of cubic regular and cubic irregular structures. The lower thickness of horizontal struts increases the porosity of cubic regular structures by 5% when compared to cubic irregular.

Quasi-static compression test

The typical stress-strain curve for cellular structures consists of three regions, linear elastic deformation followed by plastic deformation forming a plateau region and finally densification of strain takes place when the failed struts come in contact with each other. The plastic deformation and the shape of the plateau region are highly dependent on the topology and density of the material³⁰. In this study, the testing was stopped before all the struts failed and before the densification stage. This was done in order to better identify *a posteriori*; the location of the weak areas that first yielded or failed. The stress-strain curves of all the specimens are shown in Fig.5. The stress-strain curves were quite different for different topologies under monotonic testing as shown in Fig. 5a. The curve of the regular cubic structure indicates that the stress drops down to 20 MPa at very small strain, showing a catastrophic failure of struts. The failure is mainly due to buckling of vertical struts under axial loading and due to the absence of struts in other directions which introduce bending moment²⁹.

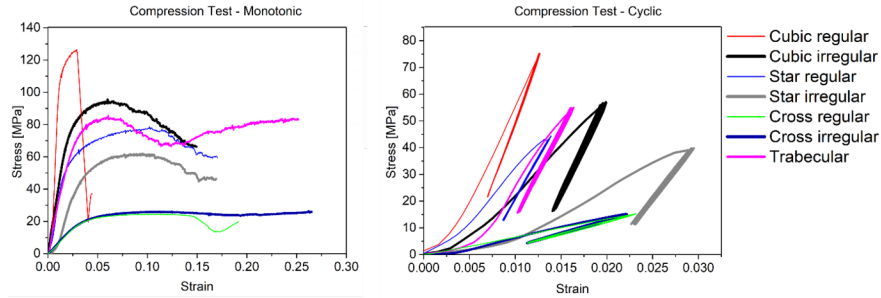


Fig.5 Compressive stress-strain curves of all specimens (a) Monotonic loading condition (b) Cyclic loading condition

This is further confirmed by the fracture plane images as shown in Fig. 6a. The cubic irregular structure has a well-defined and longer plateau compared to the cubic regular structure. This is due to the presence of inclined struts from the displaced nodes. This irregularity decreases the maximum stress that can be sustained by the structure but avoids the sudden failure of regular cubic structures. The fracture plane shown in Fig. 6b indicates a failure plane similar to a shearing band. The star-based topology structure has a plateau region similar to that of cubic irregular structures. The presence of struts in the oblique directions along with the vertical struts decreases the maximum stress that can be sustained when compared to the cubic regular structures which had struts in the vertical direction. However, the oblique struts assist in bearing the load once the vertical strut fails. While considering the star regular and star irregular stress-strain curves, the presence of irregularity has a clear effect on the stress sustained by the structures while the length of the plateau region is unaffected. It is seen from Fig.6c and 6d that the vertical struts fail, but the failure happens along a 45° shear plane.

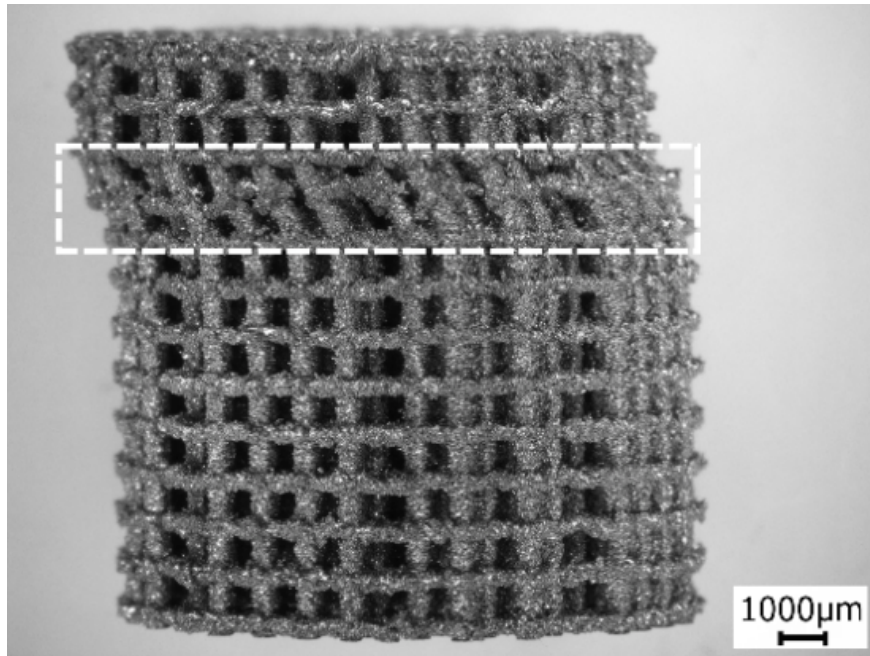


Fig.6 Fracture plane and fracture surface of specimens (XY view) subjected to compression loading along Y-direction (a) Buckling of vertical struts in cubic regular; Shear band like failure in (b) cubic irregular (c)

star regular (d) star irregular (e) cross regular (f) cross irregular; (g) failure at various locations in trabecular structures (h) SEM image indicated the formation of shear dimples at the fracture surface

The stress-strain curves for cross regular and cross irregular are completely different from the other topologies and overlap on each other. It consists of a linear region followed by a flat and long plateau which is due to the absence of struts in the vertical directions. They have the lowest stress values compared to all the other structures. The failure of the specimen took place at the junctions and experienced a shear band formation as shown in Fig. 6e and 6f⁵²⁻⁵⁴. The stress-strain curve of the trabecular structures share some properties of all kinds of topologies. It consists of a long plateau similar to the cross structures while the maximum stress value is between cubic irregular and star regular structures. The stress-strain curves clearly indicate that cubic regular samples exhibit an ideal stretching dominated behavior and cross regular and cross irregular samples exhibit an ideal bending dominated behavior.

The cyclic stress- strain curves shown in Fig.5b clearly indicate that the slope of the curve increases after the first loading cycle. This increase in stiffness after the first cycle can be due to the compaction of internal defects and plasticization at junctions which rise the overall stiffness. The specimens achieve stabilization already from the first loading cycle irrespective of the cell topology.

Table 2 Young’s Modulus and strength values

Sample	Young’s Modulus (GPa)	Young’s Modulus (GPa)	Strength (MPa)	Stren
	Monotonic E_m	Cyclic E_c	0.2% offset yield strength σ_ϕ	Maxi
Cubic regular	13.43	11.29	111	125.56
Cubic irregular	3.74	6.97	71	95.49
Star regular	4.47	6.26	48	78.66
Star irregular	2.33	4.50	36	61.92
Cross regular	0.64	0.91	17.1	24.71
Cross irregular	0.65	0.97	17.8	26.27
Trabecular	2.82	6.39	55	85.47

The Young’s modulus values and strength values are listed in Table. 2. The monotonic Young’s modulus and strength values are calculated from the linear region of the curves shown in Fig.5a. The cyclic Youngs’ modulus is calculated from the slope of the unloading part of the curve shown Fig. 5b. The cyclic modulus values are higher than the monotonic values indicating that the samples reach stabilization after the first loading cycle. Comparing the values with respect to the topology, the effect of the presence of vertical struts is clearly evident: cubic regular samples had the highest Young’s modulus followed by cubic irregular, trabecular and star-based structures. Cross-based structures with only oblique struts had the lowest stiffness. Similar conclusions can be made on the yield strength and maximum compressive strength values.

Further considerations can be made by observing how the irregularity affects the outcomes. The irregularity decreases the stiffness and strength by introducing bending dominated behavior in the structure. This effect is highly pronounced in structures having vertical struts. In cube-based structures, a decreases of 38% in cyclic modulus, 36% in yield stress and 24% in maximum stress was observed. In star-based structures, a decreases of 28% in cyclic modulus, 25% in yield stress and 21% in maximum stress was observed. In cross based structures, the irregularity had least effect with only 4-6% decrease in cyclic modulus and stress values. The modulus and the stress values of trabecular structures were similar to those of cubic irregular and star regular samples. The random orientation of the struts seems to help in terms of an isotropic distribution of load among struts.

Fatigue test

The S-N curves obtained from the fatigue tests for all the specimens are compared in Fig.7. The curve fitting parameters and the scatter in the fatigue data are as indicated in Table 3. The S-N curves clearly indicate the effect of cell topology on the fatigue behavior. As shown in Fig. 7a, cubic regular specimens represented exceptional fatigue properties and maintained their structural integrity up to 10^7 cycles under any applied load below $0.8\sigma_y$. During the experimental tests, buckling mechanism dominated the failure of cubic regular structures under compression. In this case, the absence of any sort of bending mechanism retards the fatigue crack growth³⁶. As a consequence, an expected curve is obtained by increasing the load slightly above $0.8\sigma_y$. Similar behavior that none of the specimens failed for all ranges of porosity³¹, was also reported by Yavari et al. for cubic cellular structures . By contrast, the S-N curve of cubic irregular specimens in Fig.7a indicates significantly lower fatigue strength. The effect of displacement of the nodes to induce irregularity was clearly seen and it was much more significant than the effect seen in the quasi-static compression test, where a decrease of only 24-36% of strength values was observed. The fatigue crack starts to grow at a relatively early stage because the randomly displaced nodes and the inclined struts introduce bending moments in the structure. Similar to the cubic specimens, star shaped and cross shaped specimens show lower fatigue strengths due to the irregularity, as shown in Fig. 7b and 7c. Despite the presence of vertical struts in star regular specimen, an early fatigue failure was observed when compared to the cubic specimens due to the oblique struts which induce bending moment in the specimen. Generally, a clear reduction of fatigue strength can be seen for all irregular topologies. Even though the irregularity caused a decrease of only 21-25% in the static strength values as previously evidenced in the compression test, the decrease of the S-N data points is much higher, increasing up to 80% in the the high-cycle part of the plot. However, a smaller difference between the regular and irregular topologies was observed for cross structures. Interestingly, also in static compression test the differences between regular and irregular cross-based structures were quite low. The fatigue behavior of trabecular structure Fig.7d was inferior to the regular cubic and star structures, but it was superior to the irregular cubic and star structures. The advantages of the quasi-isotropic structure induced by the randomization are more evident in this fatigue test configuration rather than in the static compression test . The S-N curves of cross based specimens show that the specimens were not able to sustain more than 10^6 cycles even at the lower range of the applied load. Therefore, the fatigue strength of all the structures were calculated at 10^6 cycles and is reported in Table. 4

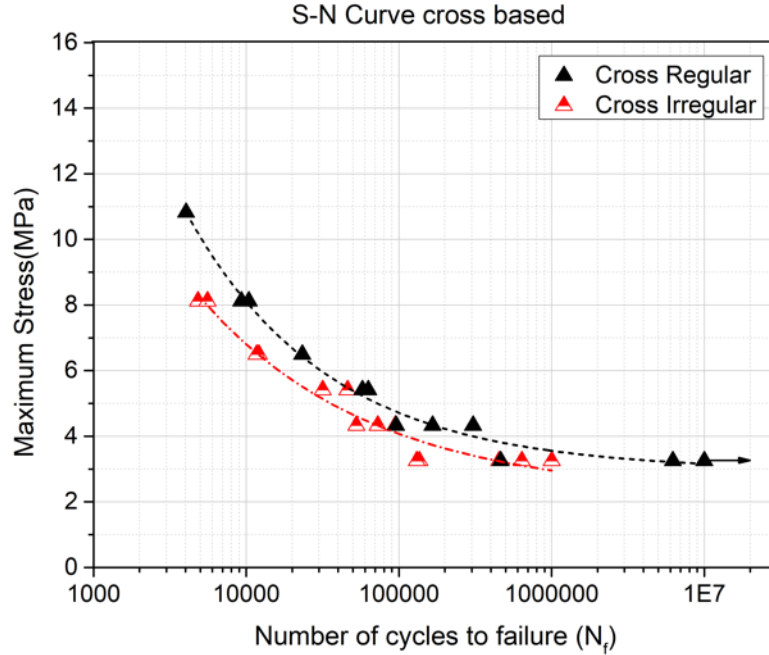


Fig.7 S-N curves for (a) Cubic based structures (b) Star based structure (c) Cross based structures (d) Trabecular

Table 3 Curve fitting parameters of fatigue test and scatter

Sample	C_1 (MPa)	C_2	m	S^2
Cubic regular	-11.34	140	0.02	136.61
Cubic irregular	1.49	658.52	0.31	7.71
Star regular	16.12	221.73	0.22	1.07
Star irregular	-1.37	286.69	0.24	9.54
Cross regular	2.95	380.64	0.47	0.07
Cross irregular	2.19	166.83	0.39	0.14
Trabecular	8.17	979.06	0.39	2.35

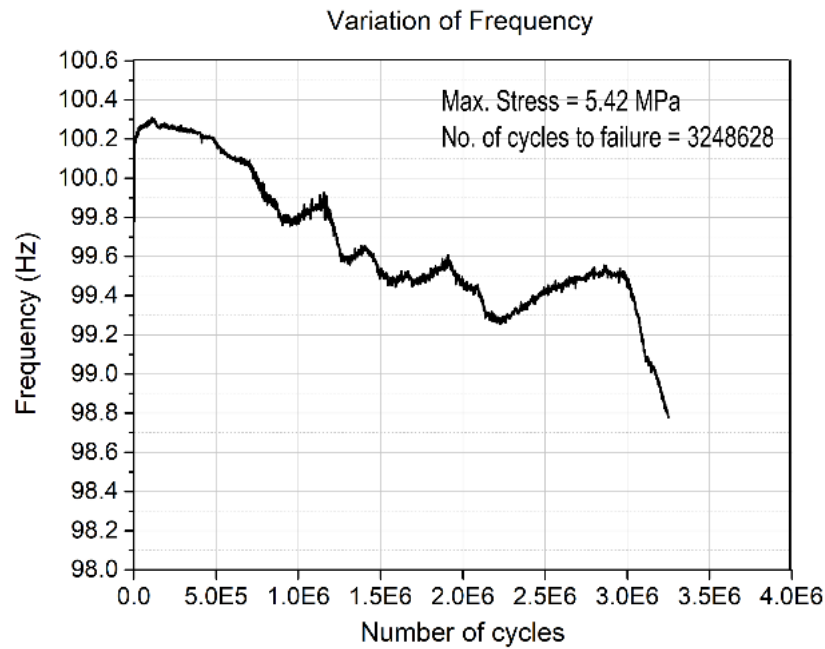
Table 4 Porosity of the samples and atigue strengths calculated at 10^6 cycles and porosity

Sample	Cubic Regular	Cubic Irregular	Star Regular	Star Irregular	Cross Regular	Cross Irregular
Porosity	76 ± 0.15	71 ± 0.21	77 ± 0.32	77 ± 0.18	79 ± 0.18	80 ± 0.19
Fatigue Strength (MPa)	100 ± 11.7	10 ± 2.8	27 ± 1.0	7.5 ± 3.1	3.5 ± 0.3	3.1 ± 0.4

Zhao et.al.³⁶ reported a fatigue strength of 75 MPa for cubic regular specimens with a porosity of $\sim 63\%$ and strut thickness of $\sim 600 \mu\text{m}$. In this study, the fatigue strength of cubic regular structure reported is 100 MPa with a porosity of $\sim 76\%$ and as-designed strut thickness of $\sim 450 \mu\text{m}$. Considering that the difference in other parameters such as microstructure and heat treatment, the estimated fatigue strength of cubic regular is similar but slightly higher when compared to Zhao et.al.³⁶. The fatigue strength of 3.1 MPa obtained from cross shaped structures is very close to the fatigue strength of 2.5MPa reported by Peng et. al.⁵⁵ from the fatigue life prediction of BCC (85% porosity) using finite element analysis. Irregularity had a predominant

impact which reduced the fatigue strength by almost ten times. Star regular specimens had the highest fatigue strength after cubic specimens. The presence of one vertical strut in star regular specimens increased the fatigue strength by almost seven times compared to cross regular. However, the same extent of increase was not seen when comparing star irregular and cross irregular since the vertical struts of the star topology are inclined with respect to the load. The fatigue strength of trabecular structures is much higher than the cross shaped samples even though they have lesser number of struts per node (4-6 trabecular and 8 cross regular). The number of struts per node for irregular cubic and star structures is also higher than in trabecular structure and yet their fatigue strength is slightly lower. The lower overall porosity of trabecular specimens has for sure an influence, but the main cause for the better behavior is the presence of struts in all the direction and the isotropy of the topology. This is further explained using the frequency variation curve in Fig.8.

The general frequency versus number of cycles curve for regular cross structure showed a linear decrease in the frequency as shown in Fig. 8a. Similar results were obtained for all regular structures and most of the irregular configuration. But some of the specimens, especially in trabecular structures, had a distinctive behavior as shown in Fig. 8b. In this case, the decrease in the frequency was not steady, as the graph indicates multiple peaks and valleys were observed which delayed the failure. The random distribution of the struts eliminates field failure, the failure occurs at the weakest link, but the random struts help in stress redistribution and the failure remains local. This can be seen through the fracture plane analysis in the next section which indicated multiple failure planes in trabecular specimens.



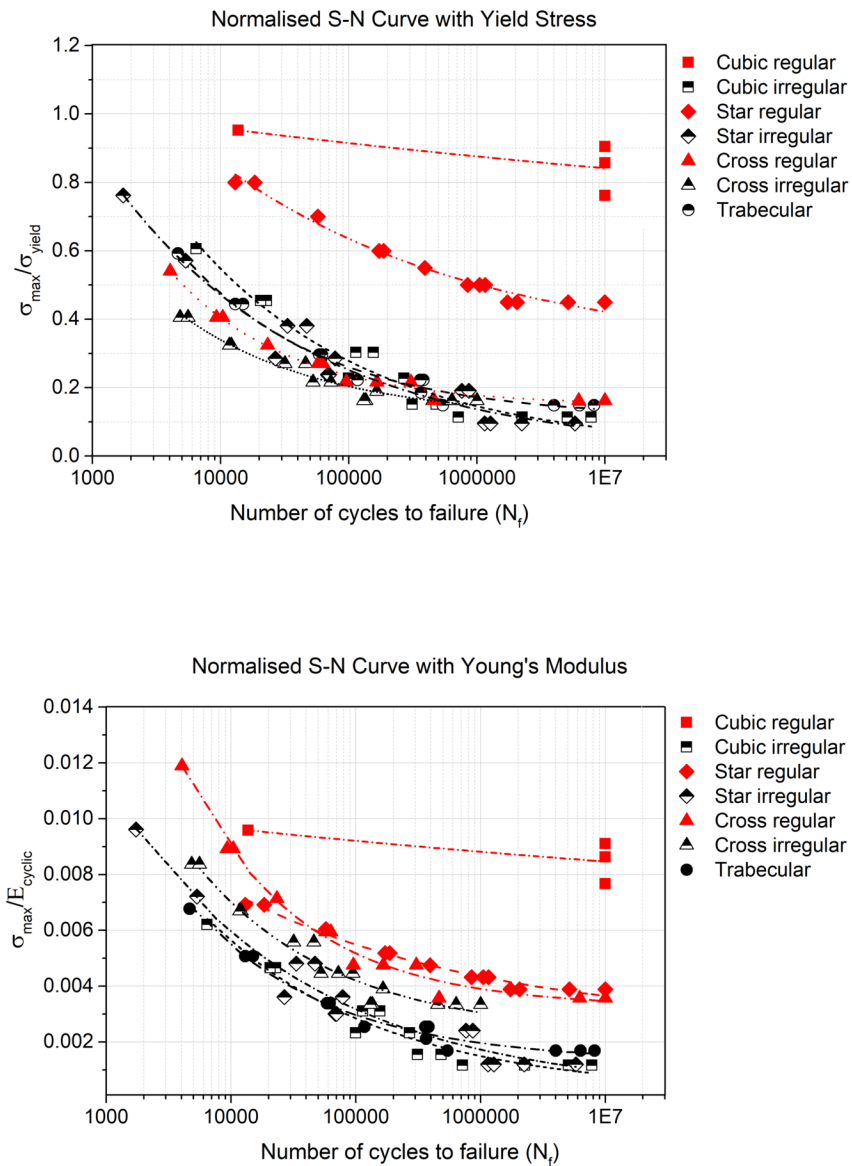


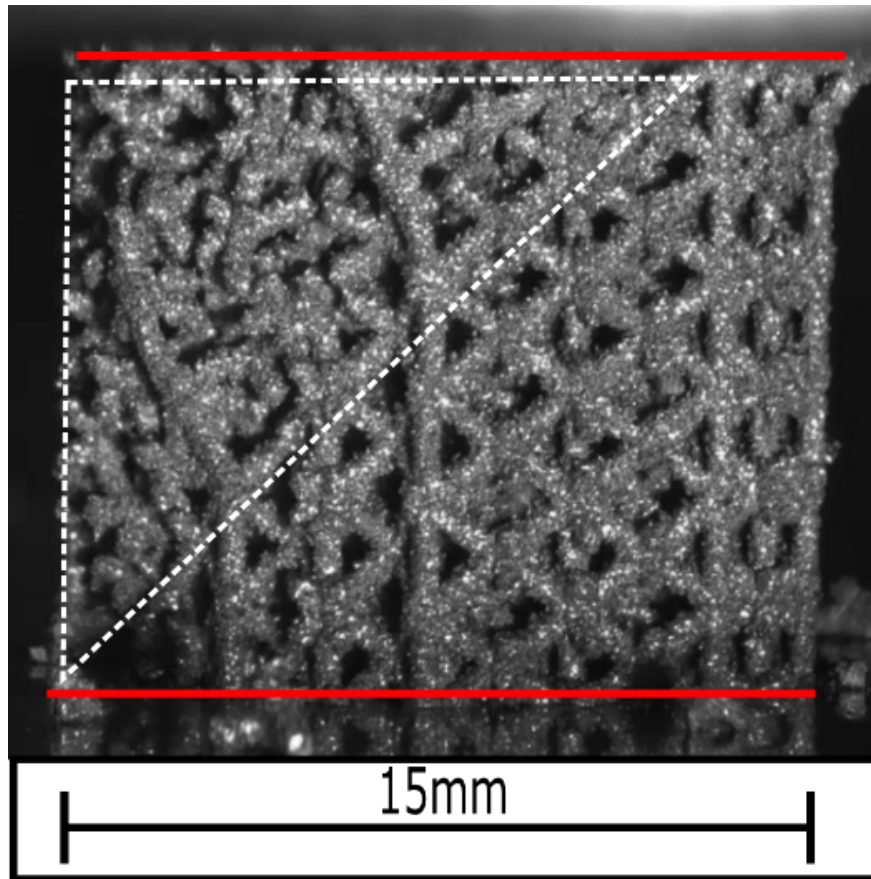
Fig.4 (a) Normalized S-N curve with yield stress (b) Normalized S-N curve with Young's modulus for all samples

Previous studies have shown that the normalized S-N curve for structures with the same topology and varying porosity fall into a single line. The effect of material is also a major factor while considering the normalized S-N curves as indicated by Ahmadi et al.³⁷. In the current study, the normalized S-N curves were obtained by using the yield strength as shown in Fig. 9a and by using cyclic Young's modulus as shown in Fig. 9b. The normalized curves of Fig.9a indicated that the three irregular configuration structures were grouped together with the trabecular structure and the purely bending dominated cross regular structure. The star regular curve was above the earlier mentioned bending dominated structures, and the cubic regular structures, purely stretching dominated, have the highest fatigue strength. Similar behavior in the normalized S-N curve was observed when comparing BCC, SC-BCC and FCC structures with simple cubic (SC) structure by Peng et

al.⁵⁵. The normalized S-N curve shown in Fig. 9b indicates that the fatigue curve of star regular and cross regular overlap with each other. While, the irregular and trabecular specimens except cross irregular have a certain overlap at the lower end of the graph. This clearly indicated the effect of irregularity in the structure leading to a decrease in the fatigue strength.

Fracture plane and Fracture surface

The fatigue fracture planes for all the topologies are shown in Fig. 10. The images have been captured from the video recorded during the compression-compression fatigue test carried out with increasing load. The fracture planes indicate the effect of topology on the failure mechanism. Cubic irregular structures were found to fail mostly due to the buckling of vertical struts in the first two layers. The failure mechanism in other topologies indicates shear bands. In star regular and cross irregular structures, the specimens failed in one plane. In cross regular structure, the failure initiated with a shear band at exactly $+45^\circ$, followed by complete compression of all the struts forming a barrel shape. In case of star irregular structure, multiple shear bands were observed at both $+30^\circ$ and -30° planes. In trabecular structures, the fracture was initiated at multiple locations leading to failure bands along more than two planes. This kind of failure supports the idea that a random distribution of struts is able to decelerate the crack propagation as observed on the frequency plot. The images also seem to indicate that the failure initiated at the junctions. This matter was further analyzed by means of SEM observations.



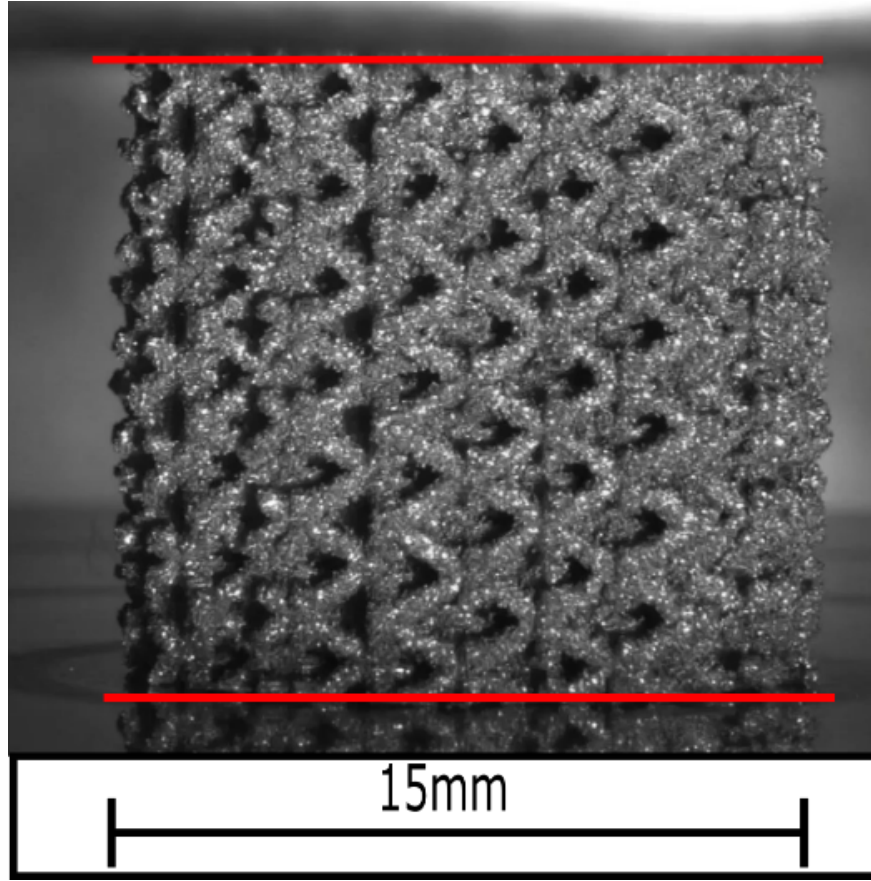


Fig.10 Before and after failure images of structures subjected to step-wise increasing load (a) and (b) cubic irregular, (c) and (d) star regular, (e) and (f) star irregular, (g) and (h) cross regular, (i) and (j) cross irregular, (k) and (l) trabecular. [Redlines indicate the location of compression plates, failure planes are highlighted using dashed lines]

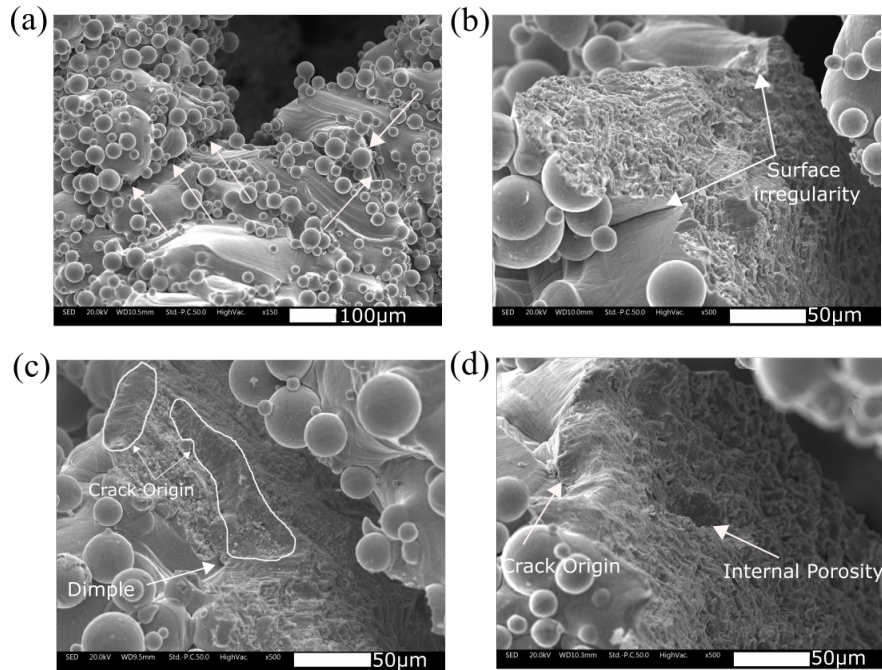


Fig.11 SEM images of fracture surface of fatigue failure locations (a) Failure at the junctions indicated with the arrows (b) Crack at locations with surface irregularity (c) Initiation of cracks at surface irregularities such as dimples and voids (d) Crack initiation at dimples and presence of internal porosity in the strut

The fatigue cracks and the fracture surface images are as shown in Fig. 11. The fatigue cracks in cellular structures usually tend to initiate at the surface of struts and at locations with high stress concentration. As shown in Fig. 11a the fatigue cracks tend to initiate at the junctions⁵⁶, the crack path also indicates that the crack has propagated along the process induced deep textures on the surface of the struts. Hrabec et al.⁵⁷ indicated that the presence of striation and textures from the AM process leads to stress concentration at critical locations leading to reduced fatigue strength. The presence of other surface irregularities such as satellite powder particle, shallow dimples and voids act as a preferential crack initiation site as indicated in Fig.11b, 11c and 11d. In the study conducted by Zhao et al.³⁶ surface dimple and unmelted powder was introduced as the source of crack initiation. Razavi et al.⁵⁸ studied the dependency of these surface irregularities to the build angle and reported significantly higher surface roughness and deeper surface defects for the surfaces printed with +45° angle with respect to the build direction. The overhanging area of the structure was reported to have higher number of partially melted powder particles therefore can be the favorable location for fatigue crack initiation. Various studies on fatigue of AM manufactured structures indicated that the presence of internal porosity and unmelted powder inside the structure influence the fatigue strength¹⁸. Fig. 11d illustrates the presence of internal porosity in one of the struts which helps in crack propagation. However, studies have also shown that the surface defects had a higher impact on the fatigue crack initiation than the internal porosity commonly present in cellular structures⁵⁹. Furthermore, the fatigue properties can be improved by chemical etching process to provide smooth surfaces, HIP treatment for reducing internal pores⁵⁹ and by having smooth junctions to avoid stress concentration⁴⁵.

Conclusion

The study focuses on the effect of various topologies on the compressive quasi-static and fatigue properties of Ti6Al4V cellular materials. Different structure topologies including trabecular based cellular material and

six different lattice based cellular materials were experimentally studied. The following conclusion can be drawn from the conducted study:

- Despite similar imposed target strut thickness and pore sizes, the fabricated specimens showed light differences in the actual porosity. Two structures possessed a porosity around 71-72%, the other five showed porosity of 76-80%. It is known that porosity influences the performances of cellular materials, however the large differences seen later in the mechanical properties can be mainly attributed to the differences in topology, rather than the small differences in porosity.
- The difference between the monotonic and cyclic Young's modulus indicates that specimens undergo stabilization and local plasticization during the initial loading of the structures.
- The Young's modulus of the cellular materials has been found to be in the range of 0.3-20 GPa, which is desirable for biomedical applications.
- Cubic structures represented the highest stiffness and strength values due to the presence of vertical struts. They have also shown excellent fatigue properties experiencing infinite fatigue lives ($>10^7$) for loads below $0.8\sigma_y$ due to the absence of bending in the struts. However, the failure appeared suddenly on a whole cross-section of the sample, much earlier with respect to the other structures
- The presence of irregularity (misalignment of nodes) has a significant effect on the quasi-static and fatigue properties of topologies with vertical struts. While the effect is quite minimal on cross shaped structures. Trabecular structures which has a fewer number of struts per node has displayed good quasi-static and fatigue properties due to the presence of struts in random directions. The random orientation of struts appears to induce a deceleration of crack propagation, avoiding the collapse of many cells at once.
- The normalized S-N curves clearly show the different behavior of the various studied structures. All the structures with irregular configuration, and trabecular were been characterized by pure a bending dominated behavior similar to cross shaped structures. The fatigue behavior of star regular structures were exactly between the stiffer, stretching dominated cubic regular structure and the other bending dominated structures due to the presence of vertical struts as well as oblique struts.
- The fatigue failure mechanism was found to be highly dependent on the cell topology. The fatigue cracks have been found to initiate at the surface irregularities such as voids, textures and dimples from the LPBF process.

Declaration of Competing Interest

The authors declared that there is no conflict of interest.

Acknowledgment

This research did not receive any specific grant from funding agencies in the public, commercial, or not-for-profit sectors.

Author Contributions

All people who meet authorship criteria are listed as authors, and all authors certify that they have participated sufficiently in the work to take public responsibility for the content, including participation in the concept, design, analysis, writing or revision of the manuscript.

Sunil Raghavendra : Writing – Original draft; Writing – review and editing; Methodology; Investigation; Formal analysis
Alberto Molinari : Supervision. **Anni Cao** : Writing – review and editing, Investigation.
Chao Gao : Writing – review and editing; Resources; Methodology. **Filippo Berto** : Writing – review and

editing Resources; Methodology; Validation. **Gianluca Zappini** : Conceptualization; Resources; Writing – review and editing; Validation. **Matteo Benedetti**: Conceptualization; Formal analysis; Methodology; Supervision; Validation.

References

- 1 Altenbach H, Oechsner A. *Cellular and Porous Materials in Structures and Processes* . Vol 521. 1st ed. (Altenbach H, Öchsner A, eds.). Vienna: Springer-Verlag Wien; 2010.
- 2 Lorna J. Gibson MFA. *Cellular Solids: Structure and Properties* . Second. Cambridge University Press; 1997.
- 3 Bobyn JD, Glassman AH, Goto H, Krygier JJ, Miller JE, Brooks CE. The effect of stem stiffness on femoral bone resorption after canine porous-coated total hip arthroplasty. *Clin Orthop Relat Res* . 1990; 196–213.
- 4 Huiskes R, Weinans H, Van Rietbergen B. The relationship between stress shielding and bone resorption around total hip stems and the effects of flexible materials. *Clin Orthop Relat Res* . 1992: 124–134.
- 5 Tan XP, Tan YJ, Chow CSL, Tor SB, Yeong WY. Metallic powder-bed based 3D printing of cellular scaffolds for orthopaedic implants: A state-of-the-art review on manufacturing, topological design, mechanical properties and biocompatibility. *Mater Sci Eng C* . 2017;76: 1328–1343.
- 6 Dabrowski B, Swieszkowski W, Godlinski D, Kurzydowski KJ. Highly porous titanium scaffolds for orthopaedic applications. *J Biomed Mater Res - Part B Appl Biomater* . 2010;95: 53–61.
- 7 Murr LE, Gaytan SM, Medina F, et al. Characterization of Ti-6Al-4V open cellular foams fabricated by additive manufacturing using electron beam melting. *Mater Sci Eng A* . 2010;527: 1861–1868.
- 8 Mark Long, Rack HJ. Titanium alloys in total joint replacement - a materials science perspective. *Biomaterials* . 1998;19: 1621–1639.
- 9 Singh, R., Lee, P.D., Dashwood, R.J., Lindley, T.C. Titanium foams for biomedical applications: a review. *Mater Technol* . 2010;25: 127–136.
- 10 Weißmann V, Drescher P, Bader R, Seitz H, Hansmann H, Laufer N. Comparison of single Ti6Al4V struts made using selective laser melting and electron beam melting subject to part orientation. *Metals (Basel)* . 2017;7.
- 11 Zhang S, Wei Q, Cheng L, Li S, Shi Y. Effects of scan line spacing on pore characteristics and mechanical properties of porous Ti6Al4V implants fabricated by selective laser melting. *Mater Des* . 2014;63: 185–193.
- 12 Qiu C, Yue S, Adkins NJE, et al. Influence of processing conditions on strut structure and compressive properties of cellular lattice structures fabricated by selective laser melting. *Mater Sci Eng A* . 2015;628: 188–197.
- 13 Sufiarov VS, Popovich AA, Borisov E V., Polozov IA, Masaylo D V., Orlov A V. The Effect of Layer Thickness at Selective Laser Melting. *Procedia Eng* . 2017;174: 126–134.
- 14 Kasperovich G, Haubrich J, Gussone J, Requena G. Correlation between porosity and processing parameters in TiAl6V4 produced by selective laser melting. *Mater Des* . 2016;105: 160–170.
- 15 Delroisse P, Jacques PJ, Maire E, Rigo O, Simar A. Effect of strut orientation on the microstructure heterogeneities in AlSi10Mg lattices processed by selective laser melting. *Scr Mater* . 2017;141: 32–35.
- 16 Ghose S, Babu S, Van Arkel RJ, Nai K, Hooper PA, Jeffers JRT. The influence of laser parameters and scanning strategies on the mechanical properties of a stochastic porous material. *Mater Des* . 2017;131: 498–508.
- 17 Wauthle R, Vrancken B, Beynaerts B, et al. Effects of build orientation and heat treatment on the microstructure and mechanical properties of selective laser melted Ti6Al4V lattice structures. *Addit Manuf*

. 2015;5: 77–84.

18 Benedetti M, Torresani E, Leoni M, et al. The effect of post-sintering treatments on the fatigue and biological behavior of Ti-6Al-4V ELI parts made by selective laser melting. *J Mech Behav Biomed Mater* . 2017;71: 295–306.

19 Pattanayak DK, Fukuda A, Matsushita T, et al. Bioactive Ti metal analogous to human cancellous bone: Fabrication by selective laser melting and chemical treatments. *Acta Biomater* . 2011;7: 1398–1406.

20 Van Hooreweder B, Apers Y, Lietaert K, Kruth JP. Improving the fatigue performance of porous metallic biomaterials produced by Selective Laser Melting. *Acta Biomater* . 2017;47: 193–202.

21 Zhang M, Yang Y, Wang D, Xiao Z, Song C, Weng C. Effect of heat treatment on the microstructure and mechanical properties of Ti6Al4V gradient structures manufactured by selective laser melting. *Mater Sci Eng A* . 2018;736: 288–297.

22 Cheng XY, Li SJ, Murr LE, et al. Compression deformation behavior of Ti-6Al-4V alloy with cellular structures fabricated by electron beam melting. *J Mech Behav Biomed Mater* . 2012;16: 153–162.

23 Amerinatanz A, Shayesteh Moghaddam N, Ibrahim H, Elahinia M. The Effect of Porosity Type on the Mechanical Performance of Porous NiTi Bone Implants. 2016: V002T06A018.

24 Xiao L, Song W, Wang C, et al. Mechanical properties of open-cell rhombic dodecahedron titanium alloy lattice structure manufactured using electron beam melting under dynamic loading. *Int J Impact Eng* . 2017;100: 75–89.

25 Ying S, Sun C, Fai K, Wei J. Materials & Design Compressive properties of functionally graded lattice structures manufactured by selective laser melting. *Mater Des* . 2017;131: 112–120.

26 Wei K, Yang Q, Ling B, Xie H, Qu Z, Fang D. Mechanical responses of titanium 3D kagome lattice structure manufactured by selective laser melting. *Extrem Mech Lett* . 2018;23: 41–48.

27 Yáñez A, Cuadrado A, Martel O, Afonso H, Monopoli D. Gyroid porous titanium structures: A versatile solution to be used as scaffolds in bone defect reconstruction. *Mater Des* . 2018;140: 21–29.

28 Zaharin HA, Rani AMA, Azam FI, et al. Effect of unit cell type and pore size on porosity and mechanical behavior of additively manufactured Ti6Al4V scaffolds. *Materials (Basel)* . 2018;11.

29 Ahmadi SM, Yavari SA, Wauthle R, et al. Additively manufactured open-cell porous biomaterials made from six different space-filling unit cells: The mechanical and morphological properties. *Materials (Basel)* . 2015;8: 1871–1896.

30 Kadkhodapour J, Montazerian H, Darabi AC, et al. Failure mechanisms of additively manufactured porous biomaterials: Effects of porosity and type of unit cell. *J Mech Behav Biomed Mater* . 2015;50: 180–191.

31 Amin Yavari S, Ahmadi SM, Wauthle R, et al. Relationship between unit cell type and porosity and the fatigue behavior of selective laser melted meta-biomaterials. *J Mech Behav Biomed Mater* . 2015;43: 91–100.

32 Parthasarathy J, Starly B, Raman S, Christensen A. Mechanical evaluation of porous titanium (Ti6Al4V) structures with electron beam melting (EBM). *J Mech Behav Biomed Mater* . 2010;3: 249–259.

33 Li SJ, Xu QS, Wang Z, et al. Influence of cell shape on mechanical properties of Ti-6Al-4V meshes fabricated by electron beam melting method. *Acta Biomater* . 2014;10: 4537–4547.

34 Ashby MF. The properties of foams and lattices. *Philos Trans R Soc A Math Phys Eng Sci* . 2006;364: 15–30.

35 Amin Yavari S, Wauthle R, Van Der Stok J, et al. Fatigue behavior of porous biomaterials manufactured using selective laser melting. *Mater Sci Eng C* . 2013;33: 4849–4858.

- 36 Zhao S, Li SJ, Hou WT, Hao YL, Yang R, Misra RDK. The influence of cell morphology on the compressive fatigue behavior of Ti-6Al-4V meshes fabricated by electron beam melting. *J Mech Behav Biomed Mater* . 2016;59: 251–264.
- 37 Ahmadi SM, Hedayati R, Li Y, et al. Fatigue performance of additively manufactured meta-biomaterials: The effects of topology and material type. *Acta Biomater* . 2018;65: 292–304.
- 38 Ghose S, Babu S, Nai K, Hooper PA, Jeffers JRT. The influence of laser parameters, scanning strategies and material on the fatigue strength of a stochastic porous structure. *Addit Manuf* . 2018;22: 290–301.
- 39 du Plessis A. Effects of process parameters on porosity in laser powder bed fusion revealed by X-ray tomography. *Addit Manuf* . 2019;30: 100871.
- 40 du Plessis A, Razavi SMJ, Berto F. The effects of microporosity in struts of gyroid lattice structures produced by laser powder bed fusion. *Mater Des* . 2020;194: 108899.
- 41 Kelly CN, Francovich J, Julmi S, et al. Fatigue behavior of As-built selective laser melted titanium scaffolds with sheet-based gyroid microarchitecture for bone tissue engineering. *Acta Biomater* . 2019;94: 610–626.
- 42 Wu MW, Chen JK, Lin BH, Chiang PH, Tsai MK. Compressive fatigue properties of additive-manufactured Ti-6Al-4V cellular material with different porosities. *Mater Sci Eng A* . 2020;790: 139695.
- 43 de Krijger J, Rans C, Van Hooreweder B, Lietaert K, Pouran B, Zadpoor AA. Effects of applied stress ratio on the fatigue behavior of additively manufactured porous biomaterials under compressive loading. *J Mech Behav Biomed Mater* . 2017;70: 7–16.
- 44 Yuan W, Hou W, Li S, et al. Heat treatment enhancing the compressive fatigue properties of open-cellular Ti-6Al-4V alloy prototypes fabricated by electron beam melting. *J Mater Sci Technol* . 2018;34: 1127–1131.
- 45 Ren D, Li S, Wang H, et al. Fatigue behavior of Ti-6Al-4V cellular structures fabricated by additive manufacturing technique. *J Mater Sci Technol* . 2019;35: 285–294.
- 46 Liu YJ, Wang HL, Li SJ, et al. Compressive and fatigue behavior of beta-type titanium porous structures fabricated by electron beam melting. *Acta Mater* . 2017;126: 58–66.
- 47 Benedetti M, Klarin J, Johansson F, et al. Study of the compression behaviour of Ti6Al4V trabecular structures produced by additive laser manufacturing. *Materials (Basel)* . 2019;12.
- 48 Cepeda-Jiménez CM, Potenza F, Magalini E, Luchin V, Molinari A, Pérez-Prado MT. Effect of energy density on the microstructure and texture evolution of Ti-6Al-4V manufactured by laser powder bed fusion. *Mater Charact* . 2020;163: 110238.
- 49 ISO 13314. ISO 13314 Mechanical testing of metals, ductility testing, compression test for porous and cellular metals. *Ref number ISO* . 2011;13314: 1–7.
- 50 Amin Yavari S, Ahmadi SM, Wauthle R, et al. Relationship between unit cell type and porosity and the fatigue behavior of selective laser melted meta-biomaterials. *J Mech Behav Biomed Mater* . 2015;43: 91–100.
- 51 Thijs L, Verhaeghe F, Craeghs T, Humbeeck J Van, Kruth JP. A study of the microstructural evolution during selective laser melting of Ti-6Al-4V. *Acta Mater* . 2010;58: 3303–3312.
- 52 Gümriük R, Mines RAW. Compressive behaviour of stainless steel micro-lattice structures. *Int J Mech Sci* . 2013;68: 125–139.
- 53 Mazur M, Leary M, Sun S, Vcelka M, Shidid D, Brandt M. Deformation and failure behaviour of Ti-6Al-4V lattice structures manufactured by selective laser melting (SLM). *Int J Adv Manuf Technol* . 2016;84: 1391–1411.

- 54 Liu X, Sekizawa K, Suzuki A, Takata N, Kobashi M, Yamada T. Compressive properties of Al-Si alloy lattice structures with three different unit cells fabricated via laser powder bed fusion. *Materials (Basel)* . 2020;13: 1–16.
- 55 Peng C, Tran P, Nguyen-Xuan H, Ferreira AJM. Mechanical performance and fatigue life prediction of lattice structures: Parametric computational approach. *Compos Struct* . 2020;235: 111821.
- 56 Boniotti L, Beretta S, Patriarca L, Rigoni L, Foletti S. Experimental and numerical investigation on compressive fatigue strength of lattice structures of AlSi7Mg manufactured by SLM. *Int J Fatigue* . 2019;128: 105181.
- 57 Hrabe NW, Heisl P, Flinn B, Körner C, Bordia RK. Compression-compression fatigue of selective electron beam melted cellular titanium (Ti-6Al-4V). *J Biomed Mater Res - Part B Appl Biomater* . 2011;99 B: 313–320.
- 58 Razavi SMJ, Van Hooreweder B, Berto F. Effect of build thickness and geometry on quasi-static and fatigue behavior of Ti-6Al-4V produced by Electron Beam Melting. *Addit Manuf* . 2020;36: 101426.
- 59 Dallago M, Fontanari V, Torresani E, et al. Fatigue and biological properties of Ti-6Al-4V ELI cellular structures with variously arranged cubic cells made by selective laser melting. *J Mech Behav Biomed Mater* . 2018;78: 381–394.